Tribol Lett (2014) 56:375–386
DOI 10.1007/s11249-014-0415-z

ORIGINAL PAPER

Boundary Layer Behaviour in Circular EHL Contacts in the Elastic-Piezoviscous Regime

C. H. Venner · N. Biboulet · A. A. Lubrecht

Received: 28 June 2014 / Accepted: 13 September 2014 / Published online: 30 September 2014

Abstract The solution of elastohydrodynamically lubricated contacts at high loads and/or low speeds can be described as a Hertzian pressure with inlet and outlet boundary layers: zones where significant pressure flow occurs. For the soft lubrication regime (elastic-isoviscous), a self-similar solution exists in the boundary layers satisfying localized equations. In this paper, the boundary layer behaviour in the elastic-piezoviscous regime is investigated. The lengthscale of the boundary layers and the scaling of pressure and film thickness are expressed in non-dimensional parameters. The boundary layer width scales as $1/\sqrt{M}$ (equivalent to $\bar{\lambda}^{3/8}$), the maximum pressure difference relative to the Hertzian solution as $1/\sqrt[3]{M}$ (equivalent to $\bar{\lambda}^{1/4}$) and the film thickness as $1/\sqrt[16]{M}$ (equivalent to $\bar{\lambda}^{3/64}$) with M the Moes non-dimensional load and $\bar{\lambda}$ a dimensionless speed parameter. The Moes dimensionless lubricant parameter L was fixed. These scalings differ from the isoviscous-elastic (soft lubrication) regime. With increasing load (decreasing speed), the solution exhibits an increasing degree of rotational symmetry. The pressure varies less than 10 % over an angle less than 45 degrees from the lubricant entrainment direction. The results provide additional fundamental understanding of the nature of elastohydrodynamic lubrication and give physical rationale to the finding of roughness deformation depending on the "inlet length". The findings may contribute to more efficient numerical solutions and to improved semi-analytical prediction methods for engineering based on physically correct asymptotic behaviour.

Keywords Thin film flows · Elastohydrodynamic Lubrication · Self-similarity

List of Symbols

a	Contact radius $a = ((3FR_x)/(2E'))^{1/3}$ (m)
d	Deformation (m)
E'	Equivalent Young's modulus $2/E' = (1-\nu_1^2)/E_1 + (1-\nu_2^2)/E_2$ (Nm^{-2})
F	External load (N)
h	Film thickness (m)
H	Dimensionless film thickness $H = hR_x/a^2$
H^*	Dimensionless film thickness $H^* = H\bar{\lambda}^{-3/5}$
H_M	Moes dimensionless film thickness $H_M = h/R_x \cdot ((\eta_0 u_s)/(E'R_x))^{-1/2}$
$\overline{H}$	Dimensionless film thickness $\overline{H} = H\sqrt[16]{M}$
ΔH	Dimensionless film thickness difference
L	Moes lubricant parameter $L = \alpha E' \cdot ((\eta_0 u_s)/(E'R_x))^{1/4}$
M	Moes load parameter point contact $M = F/(E'R_x^2) \cdot ((\eta_0 u_s)/(E'R_x))^{-3/4}$
M_l	Moes load parameter line contact $M_1 = w/(E'R_x) \cdot ((\eta_0 u_s)/(E'R_x))^{-1/2}$
p	Pressure (Nm^{-2})
P	Dimensionless pressure $P = p/p_h$
P^*	Dimensionless film thickness $P^* = P\bar{\lambda}^{-1/5}$
p_h	Maximum Hertzian pressure $p_h = (3F)/(2\pi a^2)$(Nm^{-2})

C. H. Venner (✉)
Faculty of Engineering Technology, University of Twente,
P.O. Box 217 7500, AE, Enschede, The Netherlands
e-mail: c.h.venner@utwente.nl

N. Biboulet · A. A. Lubrecht
INSA-Lyon, LaMCoS, CNRS UMR 5259, Université de Lyon,
69621 Villeurbanne, France

P_h	Dimensionless Hertzian pressure distribution $P_h = \sqrt{1 - X^2 - Y^2}$
ΔP	Dimensionless pressure difference $\Delta P = P(X, Y) - P_h$
$\overline{\Delta P}$	Dimensionless pressure difference $\overline{\Delta P} = \Delta P \sqrt[3]{M}$
r	Dimensionless radius $r = sign(X)\sqrt{X^2 + Y^2}$
R_x	Reduced radius of curvature in x $1/R_x = 1/R_{1x} + 1/R_{2x}$ (m)
Re_x	Local Reynolds number (introduction) $Re_x = u_\infty x/v$
R_y	Reduced radius of curvature in y $1/R_y = 1/R_{1y} + 1/R_{2y}$ (m)
u	Surface velocity (ms^{-1})
u_{rms}	Sum velocity $u_s = (u_1 + u_2)$ (ms^{-1})
u_∞	Freestream velocity (introduction) (ms^{-1})
w	External load per unit width (line contact) (Nm^{-1})
x	Coordinate in the direction of rolling (freestream flow) (m)
y	Coordinate perpendicular to the direction of rolling (freestream flow) (m)
x'	Coordinate in the direction of rolling (m)
y'	Coordinate perpendicular to the direction of rolling (m)
X, Y	Dimensionless coordinates $X = x/a$, $Y = y/a$
X', Y'	Dimensionless coordinates $X' = x'/a$, $Y' = y'/a$
$\overline{X}$	Dimensionless scaled coordinate $\overline{X} = \mp 1 + (X \pm 1)\sqrt{M}$
X^*	Dimensionless coordinate $X^* = (X \pm 1)\bar{\lambda}^{-2/5}$
z	Viscosity pressure index (Roelands)
α	Viscosity-pressure coefficient ($N^{-1}m^2$)
$\bar{\alpha}$	Dimensionless viscosity index $\bar{\alpha} = \alpha p_h$
η	Dynamic viscosity ($Nm^{-2}s$)
$\bar{\eta}$	Dimensionless viscosity $\bar{\eta} = \eta/\eta_0$ ($Nm^{-2}s$)
η	Boundary layer dimensionless coordinate (introduction) $\eta = y\sqrt{u_\infty/(vx)}$
v	Kinematic viscosity (introduction) $v = \eta/\rho$ (m^2s)
ϕ	Angle with X axis $\phi = \arctan(Y/X)$
$\bar{\lambda}$	Dimensionless speed parameter $\bar{\lambda} = (6\eta_0 u_s R_x^2)/(p_h a^3)$
ρ	Density (kg m^{-3})
$\bar{\rho}$	Dimensionless density $\bar{\rho} = \rho/\rho_0$
v	Poisson ratio
Δ	Dimensionless mutual approach

Subscripts

0	At ambient pressure
1, 2	Surface 1, surface 2
s	Sum
x	In x direction
y	In y direction

1 Introduction

As a result of many studies in the past decades, the behaviour of elastohydrodynamically lubricated (EHL) contacts is increasingly well understood. Advanced numerical solution methods with today's generation of computer hardware allow the solution of many realistic problems, including simulations of point contact problems with dynamic loading conditions and surface roughness passing through the contact. Based on the results of numerical solutions, formulas have been developed to predict, e.g. the film thickness for fully flooded conditions [1–4] as well as the reduction due to starvation [5, 6]. Generalized traction curves have been derived [7] and engineering models established, for the prediction of surface roughness deformation based on harmonic waviness [8–11]. These theoretical predictions were later validated experimentally [12, 13].

One of the characteristics of EHL pressure and film thickness profiles is that with increasing load and with decreasing speed, the inlet and outlet regions are narrow. This is in accordance with the fact that the solution should, in some way, approach the Hertzian solution for the dry contact. This also explains the increasing radial symmetry of the pressure in circular contacts with increasing load and/or decreasing speed [2, 14, 15]. Accurate numerical solutions for such cases require at least locally very fine meshes. This may still lead to increased computing times, in spite of the efficiency of the numerical solution method, see [16]. To optimize the computational effort, detailed understanding of the exact way in which the inlet and outlet regions are narrow in relation to the problem parameters can be beneficiary. In addition, such understanding may give new insights into modelling the transition from lubricated to dry contact from first physical principles.

The narrowing of the inlet and outlet regions in EHL problems resembles the behaviour of singular perturbation problems, which in physics are successfully analysed using the method of matched asymptotic expansions, e.g. see [17, 18]. Often there are two regions, an *inner* solution and an *outer* solution, which have different scales. In between is a transitional region referred to as "boundary layer". The length (or width, or height, depending on the type of problem) of this layer varies with the problem parameters. However, in many cases, the equations can be localized and it can be shown that there is a scaling of the variables such that a unique non-dimensional solution exists in this

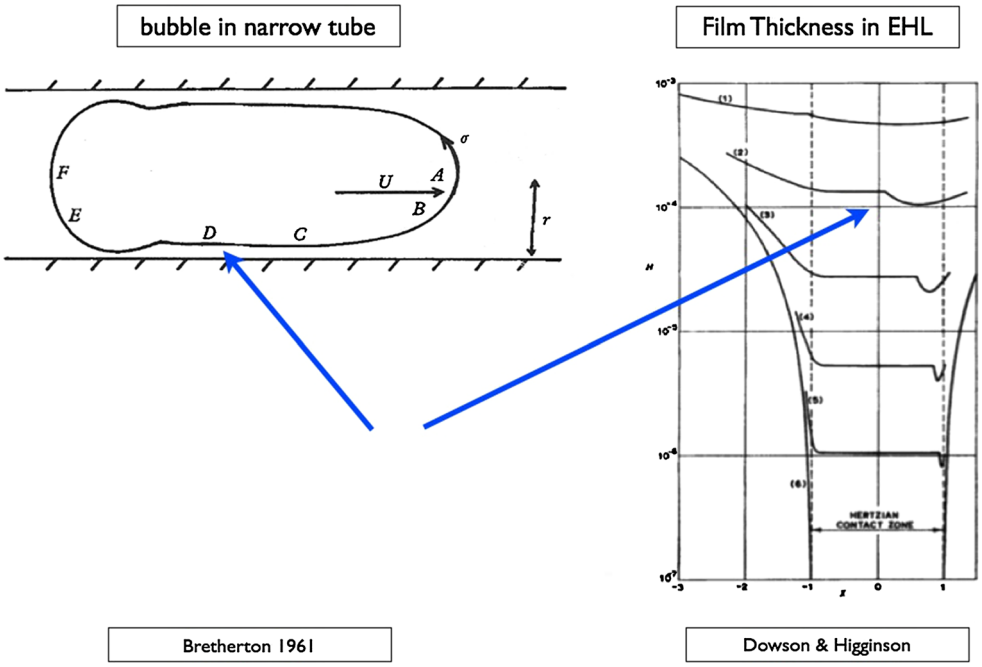

Fig. 1 Shape of narrow bubble in tube (*left*) (Bretherton [20]) and film shape in EHL contact between steel surfaces (Dowson and Higginson [21])

region. When this is the case, one speaks of a self-similar solution.

As a reminder, the terms boundary layer and self-similar solution are most well known from the problem of the flow near a wall in fluid mechanics, i.e the Blasius solution of the velocity profile in the laminar flow near a flat plate with a freestream velocity u_∞ in x direction. The velocity component along the plate $u(x,y)/u_\infty$ can be written as a function $f'(\eta)$ of only a single variable, where $\eta = y\sqrt{u_\infty/(vx)}$, and the thickness of the boundary layer behaves as $\delta/x = 4.9/\sqrt{Re_x}$, where Re_x is the local Reynolds number: $Re_x = u_\infty x/v$, see e.g [19]. However, this is not a singular perturbation problem.

A singular perturbation problem with a self-similar solution well known to the physical community is Bretherton's study of a bubble in a narrow tube [20]. The shape of the narrow gap between the bubble and the wall is strikingly similar to the film thickness solutions for EHL contacts, which were published around the same time by Dowson and Higginson [21]: nearly uniform in the centre and a downstream decrease in the film thickness, see Fig. 1. In Bretherton's study, the lubrication assumption is also used and a self-similar solution is shown to exist as is the case in many other problems in fluid mechanics and physics [22], i.e. in this case, there is a unique scaling of the solution in terms of a single parameter and the coordinate scaling is the boundary layer scale.

Several studies on elastohydrodynamic lubrication have been published in the engineering and physics literature in which the behaviour of the solution is described in terms of inlet region and outlet region, e.g. by Hooke [23], Bisset [24, 25], for line contacts, and more recently Kudish [26, 27]. In numerical studies of (harmonic) waviness passing through the contact, it was found that the deformation of the waviness depends on a single parameter, which was the same for line and point contacts, see [9]. This parameter was found to be the ratio of the wavelength of the waviness to an inlet length of the contact, which was loosely defined as the *length of the inlet pressure sweep*. In a study of the film thickness in narrow elliptic contacts, it was found that the ratio of the central to minimum film thickness was governed by exactly the same parameter [28].

Intrigued by the similarity between the Bretherton solution and the EHL solutions and the evidence of an "inlet parameter" governing many aspects of the behaviour of the problem as described above, Snoeijer et al. [29] revisited the problem of soft (highly deformed) EHL contacts in the isoviscous regime. They rigorously proved that the EHL problem can be seen as an elastic version of the Bretherton problem and that it has two similarity solutions, one on the inlet side and one on the outlet side. For the soft isoviscous case, the scaling of the inlet and outlet boundary layer is the same. For the line contact, the result generalizes the findings of Hooke [23], Herrebrugh [30], and Bisset [24, 25]. More importantly, it was shown that the solution is the same for line and point contacts, thus providing a very strong physical rationale to the empirical results of waviness deformation discussed above. The similarity solution is determined by an integro-differential equation, as opposed to the ordinary differential equations encountered in most singular fluid problems [22].

With this structure of the isoviscous heavily deformed contact clearly unraveled, the next step is to (re-)investigate the strongly deformed piezoviscous problem. The findings of the harmonic waviness deformation studies [9] suggest self-similarity in the boundary layer behaviour in this regime too. In this paper, the existence of scaling and of self-similar behaviour in the inlet and outlet layers of the piezoviscous EHL point contact problem is investigated by means of the analysis of numerical solutions.

2 EHL Equations

The equations were made dimensionless using the Hertzian parameters, see nomenclature. The non-dimensional Reynolds equation for the steady-state two-dimensional circular contact problem reads:

$$\frac{\partial}{\partial X}\left(\frac{\bar{\rho}H^3}{\bar{\eta}}\frac{\partial P}{\partial X}\right)+\frac{\partial}{\partial Y}\left(\frac{\bar{\rho}H^3}{\bar{\eta}}\frac{\partial P}{\partial Y}\right)-\bar{\lambda}\frac{\partial \bar{\rho}H}{\partial X}=0 \tag{1}$$

with $\bar{\lambda}$ defined as:

$$\bar{\lambda}=6\frac{\eta_0 u_s R_x^2}{a^3 p_h} \tag{2}$$

The density pressure relation is taken according to Dowson Higginson [31] and the Roelands [32] viscosity pressure will be used. The film thickness equation is given by:

$$H(X,Y)=-\Delta+\frac{X^2}{2}+\frac{Y^2}{2}+\frac{2}{\pi^2}\int\int\frac{P(X',Y')\,\mathrm{d}X'\mathrm{d}Y'}{\sqrt{(X-X')^2+(Y-Y')^2}} \tag{3}$$

where Δ is the (dimensionless) mutual approach, determined by the force balance equation:

$$\int\int P(X,Y)\,\mathrm{d}X\,\mathrm{d}Y=\frac{2\pi}{3} \tag{4}$$

For an incompressible lubricant and a simple exponential viscosity pressure equation, the only two dimensionless parameters appearing in the equations are $\bar{\alpha}=\alpha p_h$ and $\bar{\lambda}$.

For the case of Roelands' equation and a compressible lubricant, the values of the pressure viscosity coefficient α and the pressure viscosity index z [32] also appear. To represent load cases, the Moes dimensionless parameters will be used. These are defined as:

$$M=\frac{F}{E'R_x^2}\left(\frac{\eta_0 u_s}{E'R_x}\right)^{-3/4}\qquad L=\alpha E'\left(\frac{\eta_0 u_s}{E'R_x}\right)^{1/4} \tag{5}$$

They are related to the parameters appearing in the equation as:

$$\bar{\alpha}=\frac{L}{\pi}\left(\frac{3}{2}M\right)^{1/3}\qquad \bar{\lambda}=\left(\frac{128\pi^3}{3M^4}\right)^{1/3} \tag{6}$$

The inlet zone of a highly deformed EHL contact is the transition region between the low pressure environment and the high pressure Hertzian disc and is, in this sense, a boundary layer. The objective is now to determine whether there exist a scaling for the pressure, for the film thickness and for the length (X) coordinate such that the solutions obtained for different parameter values can all be collapsed on a single curve, the same similarity solution. Obviously, this scaling should then depend on the problem parameters, so one first needs to find out how the solution behaves in this region as a function of these parameters.

The boundary layer can be defined as the zone where the pressure flow is significant. In the piezoviscous regime, the boundary layer is limited by a small pressure gradient or by a large viscosity. No additional film variations are possible now, as the film geometry is "frozen" by the piezoviscous lubricant. Two definitions of the boundary layer were used; the first criterion determines the zone in which the pressure is significantly different from the Hertzian pressure:

$$\Delta P=\begin{cases}P-\sqrt{1-X^2-Y^2}, & \text{if } X^2+Y^2<1;\\ P, & \text{otherwise.}\end{cases} \tag{7}$$

In the same way, a film thickness difference ΔH is defined using the Hertzian dry contact deformation:

$$\Delta H=\begin{cases}H+1-r^2/2-[(2-r^2)\arcsin(1/r)+\sqrt{r^2-1}]/\pi, & \text{if } r>1;\\ H, & \text{otherwise.}\end{cases} \tag{8}$$

ΔH will be close to the central film thickness H_c in the Hertzian zone.

The second measure is the magnitude of the pressure flow related quantity $\partial P/(\bar{\eta}\partial r)$. In the central region due to the small film thickness and high viscosity, shear flow dominates, and hence, the pressure flow must be small. On the other hand, far ahead of the contact, the pressure gradient is small and the viscosity ambient, so it must also be small.

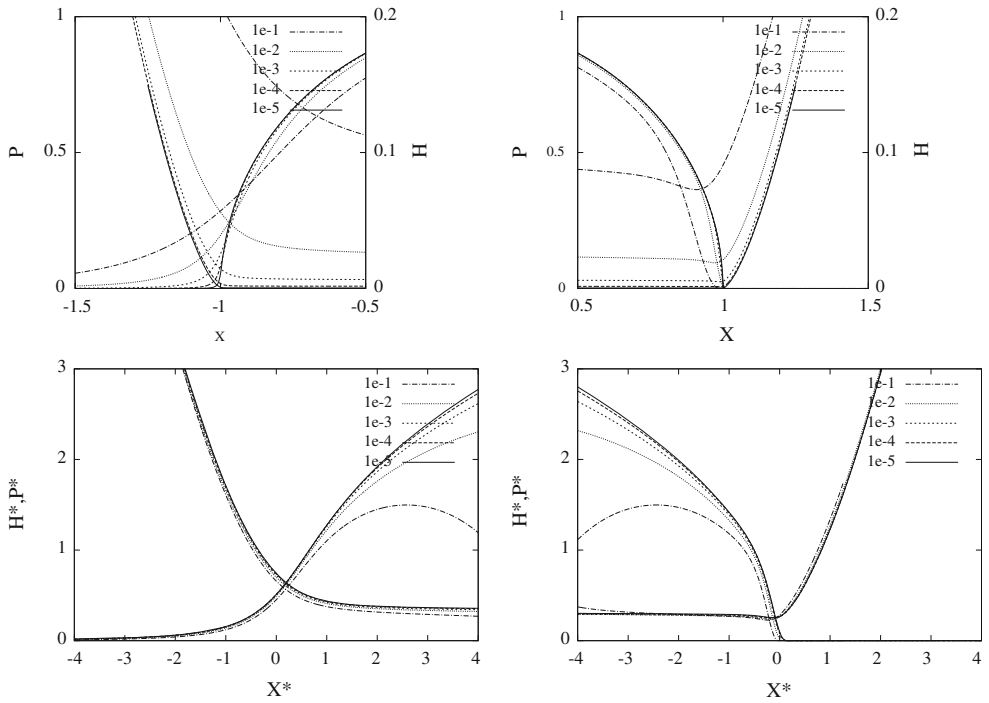

Fig. 2 Centreline dimensionless pressure P and film thickness H in the inlet (*top left*) and outlet (*top right*) regions with decreasing value of $\bar{\lambda}$. Scaled centreline pressure $P^* = P\bar{\lambda}^{-1/5}$ and $H^* = H\bar{\lambda}^{-3/5}$ as a function of scaled coordinate $X^* = X\bar{\lambda}^{-2/5}$ in inlet (*bottom left*) and outlet (*bottom right*)

Hence, it is likely to be a quantity localized in small region around the Hertzian contact circle: the boundary layer.

3 Numerical Solution

The equations were discretized on a uniform grid with second-order accuracy. The resulting discrete system of equations was solved using multilevel techniques [33, 34]. The application to the EHL point contact problem is extensively described in [35]. The efficiency of the method allows a simple and fast computation of the film thickness and pressure with very small grid spacing in a short time on a standard (personal) computers. Typical computing times for a solution of 2049^2 points are 10 min on a standard PC. The size of the computational domain for low loads must be sufficiently large. In this study for medium values of the load parameter M, the domain was taken $-4.5 \leq X \leq 1.5$ and $-3 \leq Y \leq 3$. For high M values, a smaller domain is sufficient: $-1.5 \leq X \leq 1.5$ and $-1.5 \leq Y \leq 1.5$.

4 Elastic-Isoviscous: Boundary Layer and Self-similarity

Figure 2, redrawn from [29], shows centreline profiles of the dimensionless pressure $P(X)$ and film thickness $H(X)$ for a series of loading cases of decreasing $\bar{\lambda}$ (increasing M) in the inlet and outlet regions for an isoviscous lubricant, i.e. $\bar{\alpha} = 0$ ($L = 0$). With decreasing $\bar{\lambda}$, the region over which the solution significantly differs from the Hertzian solution reduces to an increasingly narrow region near $X = \pm 1$. Also shown are the same solutions but scaled according to: $P^* = P\bar{\lambda}^{-1/5}$, $H^* = H\bar{\lambda}^{-3/5}$ as a function of $X^* = (X \pm 1)\bar{\lambda}^{-2/5}$ for the inlet and outlet, respectively. The figure shows that using this scaling of P, H and of the coordinate X, all solutions converge to a single curve in the region close to the Hertzian contact edge, i.e. $X^* \approx 0$, so there exists a single profile $P^*(X^*)$ and $H^*(X^*)$ in the inlet and outlet regions, which contains all information: the self-similar solution. Note that the scaling of the X coordinate thus exactly describes the narrowing inlet and outlet layer with decreasing $\bar{\lambda}$, and hence, it is referred to as the boundary layer length scale. For a detailed account, the reader is referred to [29]. The (dimensionless) boundary length scale is the same as the inlet length proposed by Hooke [23] and as observed by Bisset [24, 25] for the line contact problem. The film thickness solution also has the same scaling as the classic Herrebrugh solution [30]. The novelty in [29] is that this solution can be obtained from a localized equation and that it is shown to be valid for line *and* point contacts, so, for line and point contact, the scaling is the same in terms of the $\bar{\lambda}$

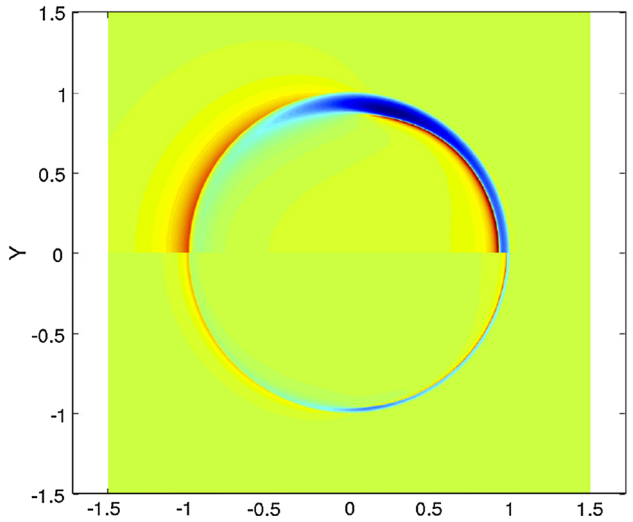

Fig. 3 Pressure difference for $M = 200$ (*top*) and $M = 2{,}000$ (*bottom*), $L = 10$

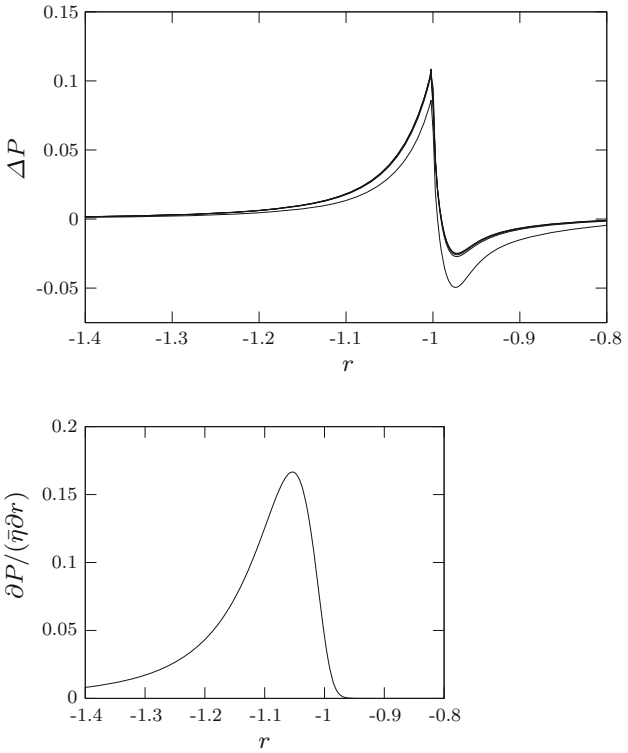

Fig. 4 Pressure difference ΔP as a function of r for $\phi = 0, 5, 10, 15, 20$ and 45 degrees (*top*) and pressure flow term as function of r for $\phi = 0$ (*bottom*). $M = 1{,}000$, $L = 10$

parameter, which reflects the same underlying physical mechanism.

In terms of the Moes dimensionless load parameter for the line contact, the dimensionless boundary layer width scales as $M_1^{-4/5}$ and the film thickness as $H_M \propto M_1^{-1/5}$, where M_1 is the Moes dimensionless load parameter for the line contact problem and H_M the Moes non-dimensional film thickness, see Nomenclature. For the point contact, the dimensionless boundary layer width scales as $M^{-8/15}$ and the scaling of the Moes dimensionless film thickness parameter is $H_M \propto M^{-2/15}$. The physical mechanism is the same, but as the Moes dimensional load parameters for the line and point contacts is not the same, this is not immediately clear from the film thickness scaling. This can now be seen as a significant drawback of the Moes non-dimensional load parameter(s), which needs to be looked into further in future research. In this study, the identification of loading cases is still done using the Moes parameter M with L fixed, and scalings found will be presented in terms of both M and $\bar{\lambda}$.

Having clarified the nature of the elastic-isoviscous (soft lubrication) problem, the objective of the present research is to (re)investigate the piezoviscous EHL problem in the regime of strong deformation and focus on boundary layer behaviour.

5 Piezo-viscous: Inlet layer

Figure 3 shows the pressure difference ΔP on the square $-1.5, 1.5$ for $M = 200$ (top) and $M = 2{,}000$ (bottom). From both figures, it can be observed that the major differences in the pressure distribution are concentrated around the unit circle $X^2 + Y^2 = 1$. Far from this circle and towards its centre, the pressure difference tends to be zero. Furthermore, it can be observed that the pressure difference as a function of the radius $r = \text{sign}(X)\sqrt{X^2 + Y^2}$ is more or less constant over an angle from $\phi = -\pi/4$ to $\phi = +\pi/4$. Note that the use of the sign(X) allows a negative value of r in the inlet and a positive value in the outlet. In terms of X, in the inlet, the pressure difference starts out positive and then becomes negative. The is also true in the outlet: first a positive then a negative difference. Hence, a transition zone is required to match these two boundary layers. For simplicity, we will define this transition zone as $\pi/4 \leq |\phi| \leq 3\pi/4$ and exclude it from our study.

Comparing the two boundary layers for the two load cases, it can be concluded that the width of the boundary layer decreases with increasing M. Furthermore, the amplitude of the pressure difference decreases with increasing M. We will now quantify some of these observations, starting with the pressure difference as a function of r for different angles ϕ, see Fig. 4. This figure apparently shows two curves, one thick line and one thin line (45 degrees). Both curves have a very similar evolution. For

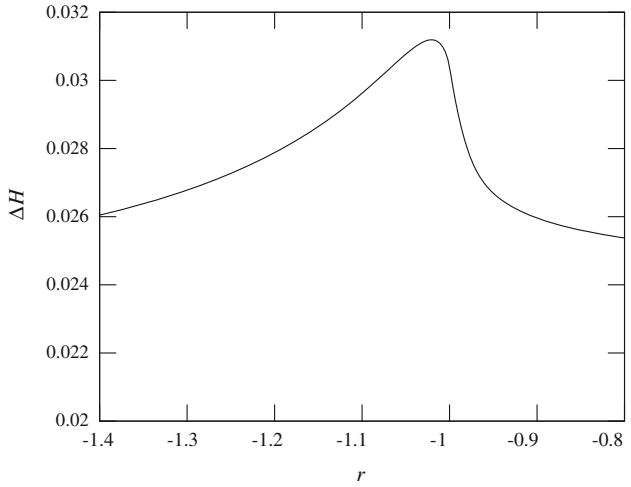

Fig. 5 Film thickness difference ΔH as a function of r for $M = 1{,}000$, $L = 10$ and $\phi = 0$ degrees

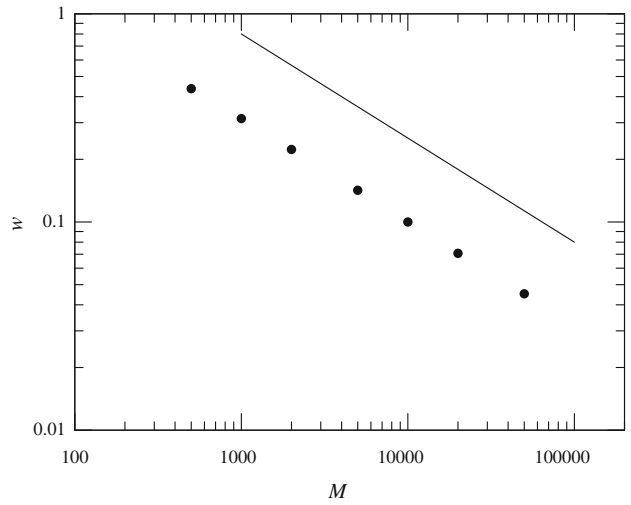

Fig. 6 Width of the inlet boundary layer as a function of M and $L = 10$, the *solid line* is a reference with a slope of $-1/2$

$r < -1$, the ΔP values are positive: in the inlet, the pressure is positive, whereas the Hertz pressure is zero. For $r > -1$, the ΔP values are negative: the total pressure is less than the Hertz pressure. The discontinuity in the slope is explained by the fact that the pressure difference compares a continuous (lubricated) and a discontinuous (Hertzian) pressure distribution, which is obviously discontinuous (at $r = -1$).

It should be noted that the thick line is not a single line, but the result of the proximity of the different curves for the angles from 0 to 20 degrees. The results for 0, 5 and 10 degrees are nearly identical, and the 15 and 20 degrees can locally be distinguished. This indicates the strong rotational symmetry of the boundary layer.

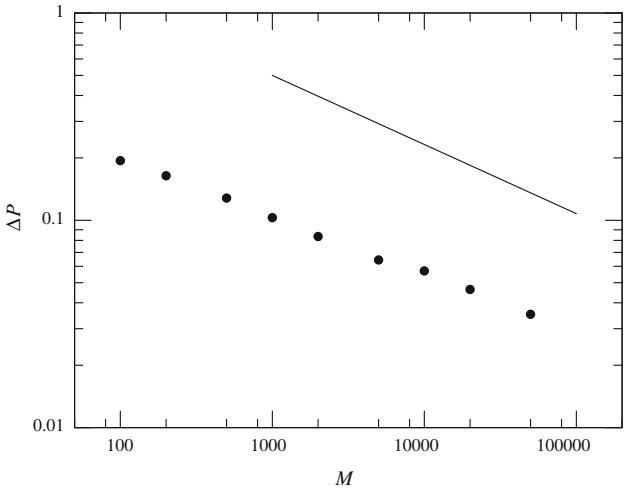

Fig. 7 Maximum pressure difference in the inlet boundary layer as a function of M and $L = 10$, the *solid line* represents a slope of $-1/3$

Figure 4 also shows the evolution of the pressure flow related term in the inlet region. It can be seen that this function is indeed only significantly different from zero in the region in which the pressure difference varies. It thus provides an equally good characterization of the boundary layer, but with the advantage that it is a continuous function. Finally, Fig. 5 shows the local deformation in the boundary layer. Because of the positive film thickness in the high pressure zone, the difference ΔH is not centred on zero, but on the central film thickness. The deformation difference, by its integral character, is smoother than the pressure difference. The local trend is a film increase, due to a local positive pressure difference.

The first boundary layer parameter that is studied is its width. The qualitative conclusion from Fig. 3 was that the width decreased with increasing M, keeping the value of the L parameter fixed ($L = 10$). The waviness amplitude reduction theory [9, 10] suggests a (non-dimensional) inlet length $\bar{\alpha}^{-3/2}L^2$ which for circular contact is the equivalent of $(\bar{\alpha}\bar{\lambda})^{1/2}$ and $\sqrt{L/M}$. For a given L, as in the present simulations, it will behave as $M^{-1/2}$: in order to define the width of the boundary layer, the pressure flow criterion was used, as it is more localized than the pressure difference criterion. The layer width is defined as the length of the region in radial direction where the pressure flow quantity exceeds 10 % of its maximum value. The analysis is performed over an angle of $-\pi/8 \leq \phi \leq +\pi/8$ with the X axis. The results are drawn in Fig. 6.

As L is fixed, the slope should theoretically be -0.5. A line with this slope is added for comparison. It can be concluded that the observed slope is exactly the same as the behaviour of the inlet length parameter previously

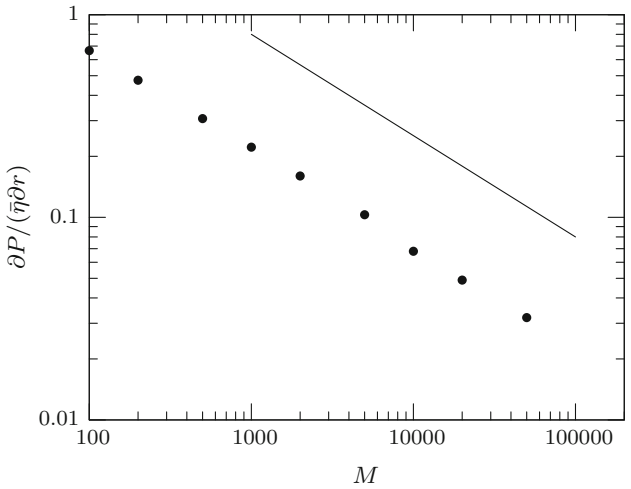

Fig. 8 Maximum pressure flow term in the inlet boundary layer as a function of M and $L = 10$, the *solid line* represents a slope of $-1/2$

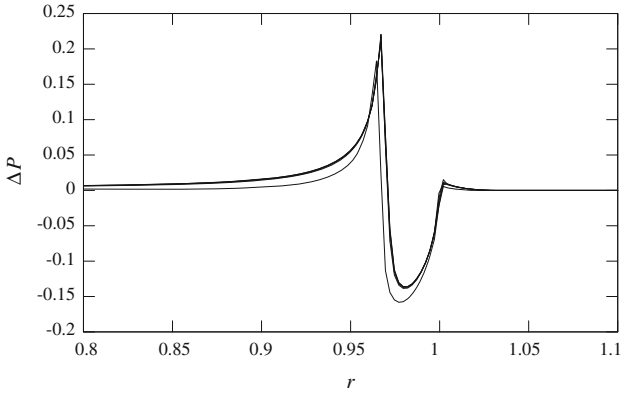

Fig. 9 Pressure difference ΔP as a function of r for $M = 1000$, $L = 10$ and $\phi = 0, 5, 10, 15, 20$ and 45 degrees

suggested. Furthermore, using the 10 % of $\partial P/(\bar{\eta}\partial r)_{\max}$ criterion, the width of the inlet boundary layer can be given as:

$$\text{inlet width} = \pi\sqrt{\frac{L}{M}} \tag{9}$$

The second boundary layer parameter studied is the maximum value of ΔP. Figure 7 shows its evolution as a function of M. As the boundary layer becomes narrower, it is to be expected that the pressure excursions tend to zero, which is indeed the case. The maximum of ΔP seems to be proportional to $1/\sqrt[3]{M}$, which is the equivalent of $\bar{\lambda}^{1/4}$. One notes some 'noise' on the maximum pressure difference value, most likely caused by the discontinuous nature of ΔP parameter. Finally, Fig. 8 shows the value of the maximum Poiseuille flow term as a function of M. This graph shows that the maximum flow scales the same as the boundary layer width and is proportional to $M^{-1/2}$.

6 Piezo-viscous: Outlet Layer

The analysis of the outlet boundary layer is slightly more difficult due to the pressure spike phenomenon. The height of this pressure spike has been the subject of many debates. Several researches have estimated that the spike is an artefact of overly simplistic numerical models. It was argued that if correct rheological and thermal models would be used, the spike height would be significantly reduced. However, Biboulet et al. [15] demonstrated that at least for conditions close to pure rolling, the measured spike height is close to the value predicted by Newtonian isothermal calculations. In [36], it is shown that for the case of a compressible lubricant using the Roelands equation for quite a number of cases, it could be shown that the spike had continuous derivative. The reason the spike occurs in the outlet and not in the inlet resides in the fact that in the outlet, the Poiseuille flow and the Couette flow are in the same direction, whereas they counteract one another in the inlet. Furthermore, the piezoviscous behaviour of the lubricant increases the pressure gradient even more in the outlet.

In Fig. 9, the pressure difference ΔP in the outlet is shown. It can be seen that the variation is very similar to the variation in the inlet, see Fig. 4. It is only because this nearly similar difference is added to the Hertzian pressure profile at different locations relative to the centre that the resulting lubricated pressure distribution appears to differ so much more from the Hertzian pressure profile. In the inlet, the ΔP singularity cancels the Hertz pressure singularity and a continuous pressure distribution results. In the outlet, the ΔP singularity occurs inside the Hertzian disc, where the Hertz pressure is still continuous, having a much stronger effect on the solution: the ensuing pressure spike.

The exit boundary layer is analysed in the same way as the inlet, and however, because of the unclear exact behaviour of the pressure spike, the $\Delta P_{\max}$ analysis is omitted. Figure 9 again reveals two curves, one thick line, which is in fact composed of several lines: the different curves representing the angles from 0 to 20 degrees. The results for 0, 5 and 10 degrees are very close, and the 15 and 20 degrees can locally be distinguished. The thin line is the result for 45 degrees which is clearly separated from the other curves. For $r < 0.97$, the ΔP values are positive: this is the pressure spike zone. For $r > 0.97$, the ΔP values are negative: the total pressure is less than the Hertz pressure. Finally, a small zone of positive values exits for $r > 1.0$; the outlet where the pressure and its derivative tend to zero, to satisfy the Reynolds cavitation condition.

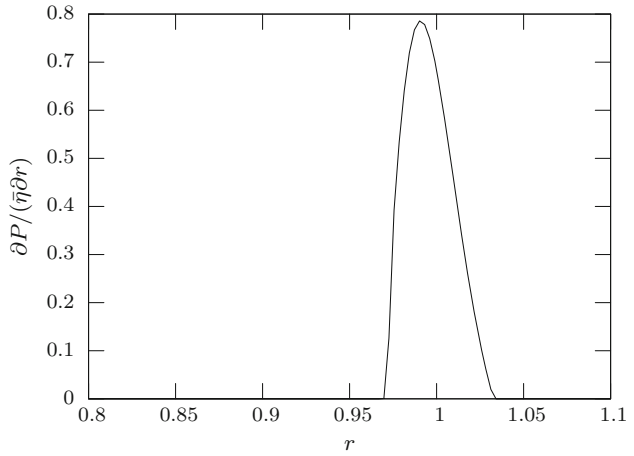

Fig. 10 Pressure flow quantity $\partial P/(\bar{\eta}\partial r)$ as a function of r for $M = 1{,}000$, $L = 10$ and $\phi = 0$ degrees

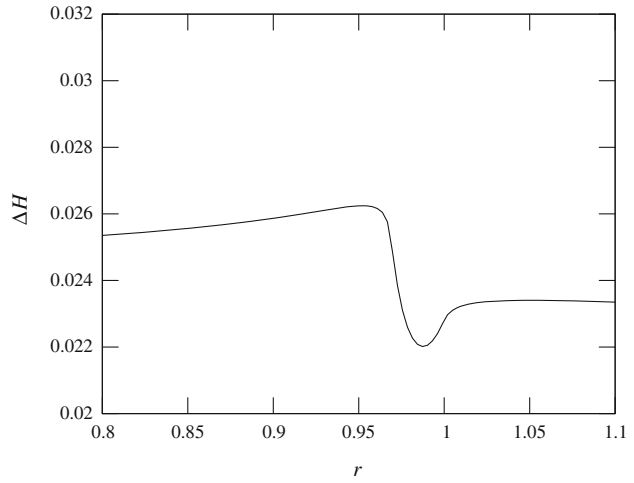

Fig. 11 Film thickness difference ΔH as a function of r for $M = 1{,}000$, $L = 10$ and $\phi = 0$ degrees

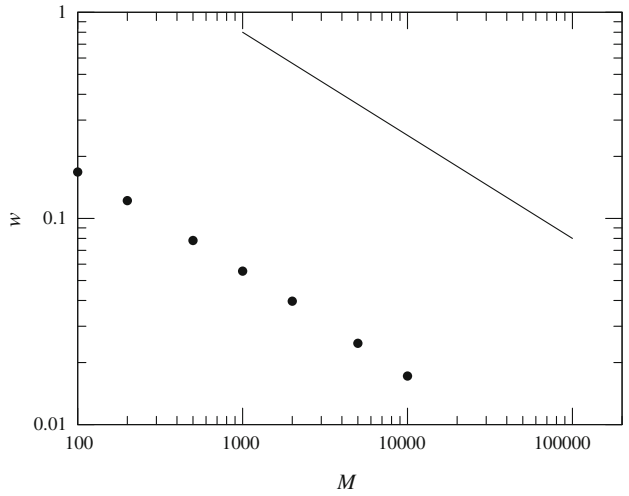

Fig. 12 Width of exit boundary layer as a function of M and $L = 10$, the *solid line* represents a slope of $-1/2$

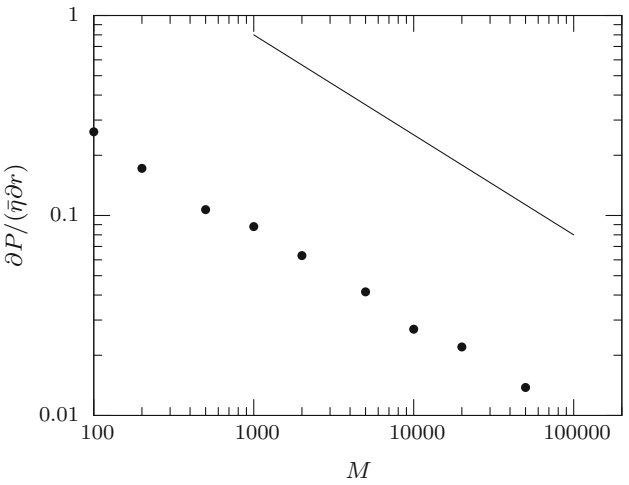

Fig. 13 Maximum value pressure flow quantity $\partial P/(\bar{\eta}\partial r)$ in the exit boundary layer as a function of M and L, the *solid line* represents a slope of -1/2

In order to facilitate the comparison of the pressure difference in the inlet and exit zone, the horizontal scale in Fig. 9 was chosen half that of Fig. 4, whereas the vertical scale was doubled in the outlet. A first conclusion is that the two curves are qualitatively very similar: a positive 'spiky' first part followed by a second negative 'rounded' part. The main differences are that the exit pressure difference excursion is larger (roughly twice) and that the width of the excursion is smaller (roughly half). Furthermore, the negative rounded pressure difference in the exit has a larger amplitude compared with the inlet zone.

Figure 10 shows that the exit boundary layer is equally well described by the pressure flow criterion and that even though the pressure difference is discontinuous (due to the pressure spike), the pressure flow quantity $\partial P/(\bar{\eta}\partial r)$ remains continuous. Please note the different axes compared with inlet pressure flow criterion shown in Fig. 4.

Figure 11 shows the local deformation in the boundary layer. Please note that the value for $r = 0.8$ is identical to the value in the inlet for $r = -0.8$ (Fig. 5). Finally, the overall deformation difference is negative, contrary to the inlet, generating the well-known minimum film thickness zone.

In order to quantify different boundary layer parameters, the analysis is performed over an angle of $-\pi/8 \leq \phi \leq +\pi/8$. This means that, as in the inlet analysis, the 45 degree results are not included!

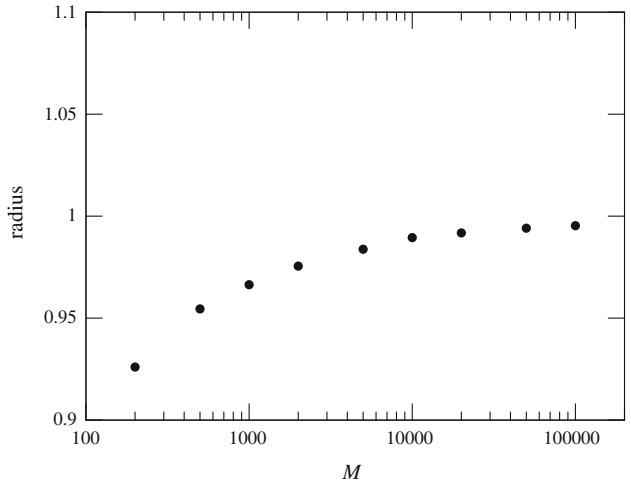

Fig. 14 Best fit radius for $\Delta P_{\max}$ as a function of M and $L = 10$

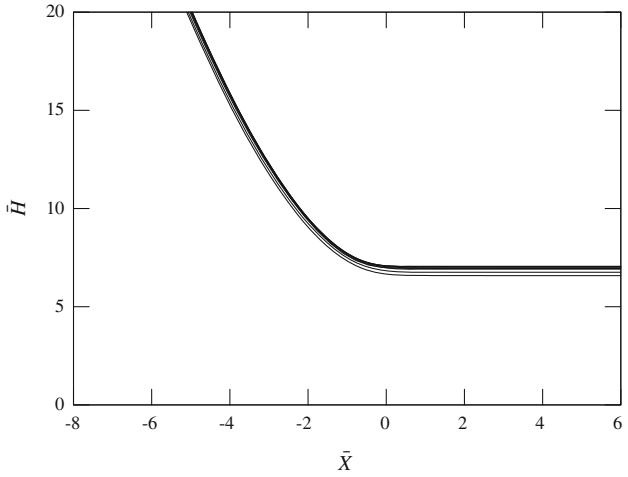

Fig. 15 Dimensionless film thickness difference $\overline{H}$ as a function of the inlet boundary layer parameter $\overline{X}$ as a function of M, $M = 100$, 200, 500 ... 10,000 and 20,000 and $L = 10$

The first boundary layer parameter that is studied is the width. The qualitative conclusion from Fig. 3 was that the width decreased with increasing M. The prediction from the amplitude reduction theory [9, 10] is that the width of the boundary layer is proportional to $\sqrt{L/M}$.

The theoretical slope of Fig. 12 should be -0.5. A straight line with this slope is added for comparison. It can be concluded that the theoretically predicted slope is indeed obtained numerically. Furthermore, the exit boundary layer is roughly six times narrower than the inlet layer, using the pressure flow criterion.

$$\text{outlet width} = 0.56\sqrt{\frac{L}{M}} \tag{10}$$

In the same way as for the inlet, also in the outlet, the maximum value of the pressure flow quantity $\partial P/(\bar{\eta}\delta r)$ has been measured. Figure 12 shows the exit boundary layer width as a function of M. With increasing M, the boundary layer narrows, and the pressure excursions should tend to zero, which is indeed the case, as shown by Fig. 13.

A last point concerning the exit boundary layer is that it is not exactly positioned on the unit circle, both its radius and centre may differ from 1.0 and 0.0, respectively. Figure 14 shows the evolution of the radius (of the $\Delta P_{\max}$ position) as a function of M. The radius value changes from 0.92 for low M values to 1.0 for high values. For even lower M values, the inlet and exit zones become large and the boundary layer concept gradually looses its interest. In fact, this is a separate regime, which can be characterized as small deformation and piezoviscous.

7 Quantitative Inlet Boundary Analysis

It has been shown in the previous sections that the pressure and film thickness distributions are radial functions in the neighbourhood of the X axis. As such, we will only study $P(X, Y = 0)$ and $H(X, Y = 0)$. We will start with a film thickness study. From the literature [2], it is known that the film thickness in the Piezoviscous Elastic regime is inversely proportional to $\sqrt[16]{M}$.

In order to quantify the dimensionless film thickness in the inlet, one uses the inlet layer width information gained in earlier sections and an $\overline{H}$ parameter defined using $\sqrt[16]{M}$:

$$\overline{X} = -1 + (X + 1)\sqrt[2]{M} \tag{11}$$

$$\overline{H} = H\sqrt[16]{M} \tag{12}$$

Figure 15 shows all film thickness profiles to be superimposed using the $\overline{H}(\overline{X})$ inlet description.

To study the pressure perturbation, a similar local pressure (difference) is defined

$$\overline{\Delta P} = \Delta P\sqrt[3]{M} \tag{13}$$

Applying these two parameters, the pressure perturbation in the inlet is plotted in Fig. 16. The pressure excursion is of order 1, whereas the width of the boundary layer is also order one. Using these local parameters, all pressure perturbations curves coincide. Figure 16 shows the results of $M = 200$, 500, 1,000, ..., 20,000. These results clearly suggest the existence of a self-similar solution in the limit of sufficiently large M. The differences for lower M values in the inlet are explained by the fact that at such low M values, the behaviour is not (yet) in the asymptotic regime. In terms of $\bar{\lambda}$, one thus finds that for a series of results obtained for fixed L parameter, one finds a (dimensionless) boundary layer width of $\bar{\lambda}^{3/8}$, a dimensionless pressure difference scaling $\Delta P \propto \bar{\lambda}^{1/4}$ and a dimensionless film

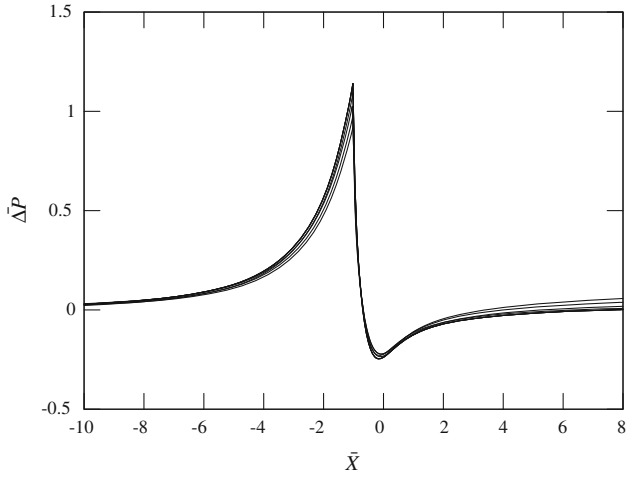

Fig. 16 Pressure difference $\overline{\Delta P}$ as a function of local coordinate $\overline{X}$ for $M = 200, 500 \ldots 10{,}000$ and 20,000 and $L = 10$

thickness scaling $\Delta H \propto \bar{\lambda}^{3/64}$. The boundary layer width and pressure scaling are not so different from the values observed for the isoviscous case. On the contrary, the power of the piezoviscous film scaling is much smaller than for the isoviscous case.

8 Conclusion

Initiated by the self-similarity observed in the solution of EHL contacts in the highly deformed isoviscous regime, this paper studies numerical solutions of the EHL circular contact to analyse boundary layer behaviour in the highly deformed piezoviscous regime. For this purpose, the pressure and film thickness difference with respect to the Hertzian solution as well as a pressure flow related measure have been used. Their dependence on the operating conditions was studied. It has been shown that for sufficiently highly loaded (deformed) contacts, these quantities are indeed localized in narrow regions on either side of the contact, thus characterizing boundary layers. It has been shown that these boundary layers exhibit a strong angular symmetry, which is consistent with the fact that the solution with increasing load should approximate the Hertzian solution. Next, the scaling of the length of the boundary layer and the solution of the pressure and film thickness inside the layer were investigated. For a given value of the Moes lubricant parameter L, the behaviour of the boundary layer width and the pressure and film thickness have been studied. It has been shown that the boundary layers on the inlet and outlet side scale in the same way.

For the case of a fixed L parameter, as was done in the present study, the non-dimensional boundary layer length scales as $\sqrt{L/M}$. The observed behaviour gives additional physical rationale to findings of the deformation of waviness and roughness patterns in EHL contacts that the amplitude reduction of waviness in EHL contacts is "inlet controlled" by a single parameter, which was deemed "length of the inlet pressure sweep". It can now be seen that in physical terms, this is in fact the lengthscale of the boundary layer. The present simulations carried out for fixed $L = 10$ give in terms of the $\bar{\lambda}$ parameter a scaling of $\bar{\lambda}^{3/8}$, where for $L = 0$, the isoviscous case $\bar{\lambda}^{2/5}$ was found.

Using local coordinates $\overline{\Delta P}(\overline{X})$ for the inlet, it was shown that a non-dimensional pressure difference in the inlet is independent of M for heavily loaded/deformed EHL contacts. Similarly, a dimensionless film geometry $\overline{H}(\overline{X})$ is obtained, which is also independent of M. This indicates the existence of self-similar pressure and film profiles in this region. The observed behaviour suggests for the present results with fixed $L = 10$ a pressure scaling $\bar{\lambda}^{1/4}$ and a film scaling $\bar{\lambda}^{3/64}$.

Future work should study if and how this self-similar solution can be obtained from localized equations. The observed similarity between the ΔP profile in the inlet and outlet region can be investigated further to clarify the elusive pressure spike behaviour. Also, the influence of the L parameter should be analysed in detail, in spite of its limited range of values that it takes in applications where the piezoviscous regime roughly starts for $L = 5$ and $L = 20$ which seems to be a limit for many practical applications.

In addition to clarifying the fundamental physical nature of the EHL problem, it is anticipated that the results, as presented in this paper, will contribute to improved and new semi-analytic engineering tools for the prediction of EHL contact behaviour. The results can also help to optimize numerical simulations and to reduce the need for full numerical simulations of transient two-dimensional contacts.

References

1. Dowson, D., Higginson, G.R.: New roller-bearing lubrication formula. Engineering **192**(4972), 158–159 (1961)
2. Hamrock, B.J., Dowson, D.: Isothermal elastohydrodynamic lubrication of point contacts, part III, Fully flooded Results. ASME J. Lubr. Technol. **99**, 264–275 (1977)
3. Chittenden, R.J., Dowson, D., Dunn, J.F., Taylor, C.M.: A theoretical analysis of the isothermal elastohydrodynamic lubrication of concentrated contacts I. direction of lubricant entrainment coincident with the major axis of the Hertzian contact Ellipse. Proc R Soc Lond A **397**, 245–269 (1985)
4. Nijenbanning, G., Venner, C.H., Moes, H.: Film thickness in elastohydrodynamically lubricated elliptic contacts. WEAR **176**, 217–229 (1994)

5. Chevalier, F., Cann, P.M.E., Colin, F., Dalmaz, G., Lubrecht, A.A.: Film thickness in starved EHL point contacts. ASME J. Tribol. **120**(1), 126–133 (1996)
6. Damiens, B., Venner, C.H., Cann, P.M.E., Lubrecht, A.A.: Starved lubrication of elliptical EHD contacts. ASME J. Tribol. **126**(1), 105–111 (2004)
7. Jacod, B., Venner, C.H., Lugt, P.M.: A generalized traction curve for EHL contacts. ASME J. Tribol **123**, 248–253 (2003)
8. Greenwood, J., Morales-Espejel, G.E.: The behaviour of transverse roughness in EHL contacts. Proc. IMechE J. Eng. Tribol. **208**, 121–132 (1994)
9. Hooke, C.J., Venner, C.H.: Surface roughness attenuation in line and point contacts. Proc. Inst. Mech. Eng. J. Eng. Tribol. **214**, 439–444 (2000)
10. Venner, C.H., Lubrecht, A.A.: An engineering tool for the quantitative prediction of general roughness deformation in EHL contacts based on harmonic waviness attenuation. Proc. ImechE. Part J: J. Eng. Tribol. **219**, 303–312 (2005)
11. Masen, M.A., Venner, C.H., Lugt, P.M., Tripp, J.H.: Effects of surface micro-geometry on the lift-off speed of an EHL contact. STLE Tribol. Trans. **45**(1), 21–30 (2002)
12. Glovnea, R.P., Choo, J.W., Olver, A.V., Spikes, H.A.: Compression of a single transverse ridge in a circular elastohydrodynamic contact. ASME J. Tribol. **125**, 275–282 (2003)
13. Sperka, P., Krupka, I., Hartl, M.: Experimental study of real roughness attenuation in concentrated contacts. Tribol. Int. **43**, 1893–1901 (2010)
14. Venner, C.H., ten Napel, W.E.: Multilevel solution of the elastohydrodynamically lubricated circular contact problem, part II: Smooth surface results. WEAR **152**, 351–367 (1992)
15. Biboulet, N., Sperka, P., Venner, C.H., Lubrecht, A.A., Krupka, I.: Obtaining the pressure spike and maximum shear stress from optical interferometry data. Tribol. Int. **62**, 1–7 (2013)
16. Mora, F., Sainsot, P., Le Chenadec, Y., Lubrecht, A.A.: Lubrication of 2D soft elastohydrodynamic contacts: extension of the amplitude reduction theory. Proc. Inst. Mech. Eng. **226**, 769–774 (2012)
17. Howison, S.: Practical applied mathematics: modelling, analysis, approximation, Cambridge University Press, Cambridge, UK, ISBN 139780521842743 (2005)
18. Holmes, M.H.: Introduction to perturbation methods, Springer, text in applied mathematics, 20, Springer, New York, USA. ISBN 9781461454762 (1995).
19. Schlichting, H., Gersten, K.: Boundary-Layer Theory, McGraw Hill, New York, USA, ISBN 978-3-540-66270-9 (2000).
20. Bretherton, F.P.: The motion of long bubbles in tubes. J. Fluid Mech. **10**, 166–188 (1961)
21. Dowson, D., Higginson, G.R.: The effect of material properties on the lubrication of elastic rollers. J. Mech. Eng. Sci. **1**(1), 6–15 (1960)
22. Eggers, J., Fontelos, M.A.: The role of self-similarity in singularities of partial differential equations. Nonlinearity **22**, R1–R44 (2009)
23. Hooke, C.J.: The elastohydrodynamic lubrication of heavily loaded contacts. J. Mech. Eng. Sci. **19**(4), 149–156 (1977)
24. Bisset, E.J.: The line contact problem of elastohydrodynamic lubrication. I. Asymptotic structure for low speeds. Proc. Roy. Soc. Lond. **A 424**, 393–407 (1989)
25. Bisset, E.J.: The line contact problem of elastohydrodynamic lubrication. II. Numerical solution of the integrodifferential equations in the transition and exit layers. Proc. Roy. Soc. Lond. **A424**, 409–429 (1989)
26. Kudish, I.I., Covitch, M.J.: Modeling and Analytical Methods in Tribology. Chapman and Hall/CRC, Boca Raton (2010)
27. Kudish, I.I.: Asymptotic analysis of lubricated heavily loaded point contacts. Lub. Sci. (2013)
28. Venner, C.H., Lubrecht, A.A.: Revisiting film thickness in slender EHL contacts. Proc. ImechE. Part C: J. Mech. Eng. Sci. **224**, 2549–2558 (2010)
29. Snoeijer, J.H., Eggers, J., Venner, C.H.: Similarity theory of lubricated Hertzian contacts. Phys. Fluids **25**, 101705 (2013)
30. Herrebrugh, K.: Solving the incompressible and isothermal problem in elastohydrodynamic lubrication through an integral equation. ASME J. Tribol. **90**, 262–270 (1968)
31. Dowson, D., Higginson, G.R., Whitaker, A.V.: Elastohydrodynamic lubrication: a survey of isothermal solutions. J. Mech. Eng. Sci. **4**(2), 121–126 (1962)
32. Roelands, C.J.A., Correlational aspects of the viscosity-temperature-pressure relationship of lubricating oils, PhD. Thesis, Technical University Delft, The Netherlands (V.R.B. Groningen, The Netherlands) (1966).
33. Brandt, A.: Multi-Level adaptive Solutions to boundary value problems. Math. Comp. **31**(2), 333–390 (1977)
34. Brandt, A., Lubrecht, A.A.: MultiLevel matrix multiplication and fast Solutions of integral equations. J. Comp. Phys. **90**(2), 348–390 (1990)
35. Venner, C.H. and Lubrecht, A.A.: MultiLevel methods in lubrication, Elsevier Tribology Series, 19 (2000)
36. Venner, C.H., ten Napel, W.E.: Numerical calculation of the pressure spike in elastohydrodynamic lubrication. Lubr. Sci. **2**(4), 321–335 (1990)